Research Article Wiley Online Library ELECTROANALYSIS

doi.org/10.1002/elan.202100672

Electrochemical Immunosensor Made with Zein-based Nanofibers for On-site Detection of Aflatoxin B1

Danilo M. Dos Santos[+],*[a] Fernanda L. Migliorini[+],[a] Andrey C. Soares,[a] Luiz H. C. Mattoso,[a] Osvaldo N. Oliveira, Jr.,[b] and Daniel S. Correa*[a]

Abstract: A disposable electrochemical immunosensor for on-site detection of aflatoxin B1(AFB1), one of the most toxic mycotoxins in agri-food products, was fabricated through a low-cost cut-printing method and then modified with zein/polypyrrole(PPy) electrospun nanofibers onto which anti-AFB1 monoclonal antibodies were immobilized covalently. Fabrication was possible with an innovative and simple approach to adsorb nanofibers onto the working electrode during electrospinning. Electrochemical impedance spectroscopy was employed as the principle of detection, and the data collected with a portable potentiostat were treated with information visualization techniques. The nanostructured immunosensor showed a high sensitivity for AFB1 with a linear detection range from 0.25 to 10 ng mL^{-1} and a theoretical limit of detection of 0.092 ng mL^{-1}, which is adequate to detect AFB1 in food, according to regulatory agencies.

Keywords: electrospun fibers · immunosensors · food contaminants · electrochemical impedance · aflatoxin B1

1 Introduction

On-site detection of food contaminants and pollutants in water has become an important goal to pursue, sparking considerable research into novel materials for sensing and devices [1,2]. The requirements for such detection are stringent as the sensing platforms need to be low cost, portable, and provide high sensitivity, selectivity and rapid response. Depending on the application there is the additional requirement of biocompatibility and/or biodegradability. Various materials - and methods to produce them – have been investigated, along with suitable techniques for efficient detection of different analytes (for reviews on these subjects, see ref. [3–6]). Electrochemical sensors and biosensors have proven adequate to provide results for on-site detection [1,2,7,8], but successful cases inevitably demanded a judicious choice of materials and measuring principles. For biosensors, in particular, the matrix onto which the active layer is deposited must be suitable to preserve the activity of biomolecules and assist in generating a large electrochemical signal [2,7].

Recently, special attention has been given to electrochemical sensors fabricated via printing deposition of single or multiple layers of graphite-based conductive inks onto a waterproof substrate [9–11]. The appealing features of such constructs include good sensing performance, low cost, ease of preparation, and sustainability [12]. In addition, the sensing performance can be enhanced with incorporation of nanomaterials such as metallic nanoparticles [13], reduced graphene oxide [14], multiwalled carbon nanotubes [15], and electrospun nanofibers. The latter are promising for biosensors [16–18] for two main reasons. First, their morphology, composition, electrical properties, and structure can be modulated. The other reason is related to their high surface area/volume ratios, which provide numerous sites for immobilization of recognition elements to yield an efficient analyte-surface interaction. Indeed, the high porosity of electrospun fibers permits increased accessibility and offers low mass transport resistance, thus enhancing the analyte diffusion through the sensing layer [19,20]. The main challenge now is to adsorb electrospun nanofibers directly onto the working electrode during electrospinning.

In this paper, we report on a simple strategy to modify working electrodes with electrospun zein/polypyrrole (PPy) nanofibers onto which a layer of antibodies could be immobilized covalently. The protein extracted from corn zein was used here as polymeric matrix for its biodegradability, low cost, and high availability. Also, zein has reactive functional groups, including primary amine (–NH_2) and primary and secondary hydroxyl groups (–OH), which are useful to attach antibodies [21–23]. The semiconducting polymer PPy [24] was blended with zein to confer electrical properties to the electrospun nanofibers. The platform was used to detect aflatoxin B1

[a] D. M. Dos Santos,[+] F. L. Migliorini,[+] A. C. Soares, L. H. C. Mattoso, D. S. Correa
Nanotechnology National Laboratory for Agriculture (LNNA), Embrapa Instrumentação, 13560-970 São Carlos, SP, Brazil
E-mail: martinsdanilo.9@gmail.com
daniel.correa@embrapa.br
[b] O. N. Oliveira, Jr.
São Carlos Institute of Physics, University of São Paulo, P.O. Box 369, São Carlos 13560-970, SP, Brazil
[+] These authors contributed equally to this work.

Supporting information for this article is available on the WWW under https://doi.org/10.1002/elan.202100672

(AFB1), a metabolite produced by *Aspergillus flavus* and *Aspergillus parasitic*, a common food-contaminating mycotoxin which threats humans and animals due to its carcinogenic, teratogenic, and immunosuppressive nature [25–27]. This contaminant is resistant to thermal and chemical treatment, being found in such food products as corn, barley, nut, bean, oils, rice, fruits, and milk [28,29]. AFB1 is normally detected with high-performance liquid chromatography (HPLC) [30], liquid chromatography-mass spectrometry (LC–MS) [31], and enzyme-linked immunosorbent assay (ELISA) [32], which are time-consuming, expensive and are unsuitable for on-site rapid analysis. Detection of AFB1 has also been made with electrochemical biosensors [15,27,33], including in our previous work where a simple, low-cost cut-printing method was used to produce the electrodes [15]. Herein, we take advantage of the versatility of the generic platform to obtain a portable and ultrasensitive electrochemical immunosensor to detect AFB1 in food samples. A hand-held commercial potentiostat was successfully used to on-site detection of AFB1 via electrochemical impedance spectroscopy by using the nanofiber-based electrochemical immunosensor, which improved AFB1 detection including in features as lower limit of detection, higher selectivity, and stability.

2 Experimental Details

2.1 Materials

Zein ($(\overline{Mw}) = 24{,}000$ g mol^{-1}), polypyrrole (PPy), aflatoxin B1, Anti-AFB1 antibody, ochratoxin A, *N*-Ethyl-*N*'-(3-dimethyl aminopropyl) carbodiimide hydrochloride (EDC), *N*-hydroxyl succinimide (NHS) and 2-(N-morpholino) ethanesulfonic acid (MES) buffer were purchased from Sigma-Aldrich. Shellac was purchased from Acrilex® (São Bernardo do Campo/SP, Brazil), while graphite and carbon black were acquired from Synth (Diadema/SP; Brazil) and Cabot (Boston/Massachusetts; USA), respectively. Adhesive paper was used as substrate from PIMACO (A4 ink-jet/laser 288.5×200.0 367 BIC, Brazil) and crystal acetate sheet used as a substrate for placing adhesive paper (Artigianato A4, Brasil).

2.2 Nanofiber-based Electrochemical Immunosensor Fabrication

A schematic diagram with the steps for the fabrication of nanofiber-based electrochemical immunosensor is given in Figure 1. The disposable electrodes were prepared using a simple, low-cost cut-printing process with slight modifications to the methodology described in a previous work [15]. A thin layer of conductive ink made of a suspension of graphite/carbon black powder (90/10 (w/w))

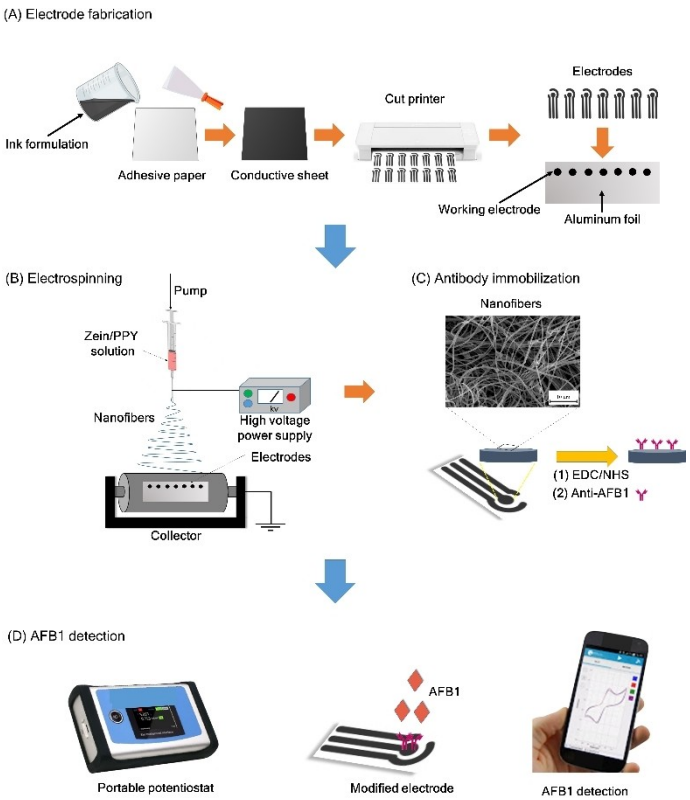

Fig. 1. Preparation of nanofiber-based electrochemical immunosensor: (A) Fabrication of the cut-printed electrode made of conductive ink; (B) electrospinning onto the working electrode; (C) immobilization of anti-AFB1 onto nanofiber surface; (D) electrochemical detection of AFB1 using a hand-held potentiostat.

in shellac in a proportion of 30 % (w/w) was homogeneously deposited onto the adhesive paper (Figure 1A) and then dried at 40 °C for 1 h in an air-circulating oven. A cut printer (Silhouette, model 3, Moema/SP, Brazil) was used to cut a mask with working (diameter = 3.3 mm), counter, and reference electrodes from the as-prepared conductive sheets. The mask was removed and glued onto a flexible and waterproof acetate sheet, yielding the sensing platform in Figure 1A. The functionalization of the working electrode depicted in Figure 1B was made with the electrospinning method. A zein solution in acetic acid at 30 % (w/v) was diluted by adding 5 % aqueous polypyrrole (PPy) solution to result in 24 % (w/v) and 1 % (w/v) of zein and PPy, respectively. This formulation was optimized in subsidiary experiments (not shown). Electrospinning was carried out using a flow rate of 0.5 mL h^{-1}, a working distance of 8 cm, and applied voltage of 22 kV. The reference electrodes were previously covered by an aluminum foil and fibers were directly electrospun only onto the working electrode attached to a stainless-steel drum collector. The fiber deposition was carried out for 7 min at 25 ± 3 °C and relative humidity of 40 %. After electrospinning, the modified electrodes were carefully removed from the aluminum foil and stored in a desiccator before further use.

The immobilization of anti-AFB1 antibodies onto the electrospun nanofibers surface was performed in the three stages depicted in Figure 1C. First, 20 µL of EDC (0.8 mol L^{-1})/NHS (0.2 mol L^{-1}) in 0.1 mol·L^{-1} MES buffer was deposited onto the modified electrode and kept for 40 min at 25 °C. The activated electrode surface was washed with PBS (pH 7.4) and dried at room temperature. Sequentially, 10 µL of anti-AFB1 solution (100 µg mL^{-1}) in 0.1 mol·L^{-1} MES buffer was poured over the activated electrode and maintained for 40 min at 25 °C to promote covalent attachment of antibodies to the nanofibers. The electrode was then washed with PBS to remove unbound antibodies and dried, followed by adding 10 µL of 5 mg mL^{-1} BSA solution for 30 min at 25 °C to block non-active sites [34,35]. The modified electrode was finally rinsed with PBS and stored at 4 °C until use.

2.3 Morphological and Spectroscopic Characterization of the Sensing Platforms

The morphology of the working electrode and nanofibers was assessed with a scanning electron microscope (SEM, JEOL 6510) using an acceleration voltage of 10kV after sputter coating the samples with gold. The fiber average diameter was determined from the SEM images using ImageJ 1.45 software (National Institutes of Health, Bethesda, MD, USA) from at least 100 fibers chosen randomly. Polarization-modulated infrared reflection absorption spectroscopy (PM-IRRAS) was used to investigate the interactions between electrospun nanofibers and anti-AFB1, in addition to the AFB1 detection mechanism. The measurements were performed in a PMI 550 spectrophotometer (KSV Instruments) at an incidence angle of 81° and spectral resolution of 8 cm^{-1}.

2.4 Electrochemical Detection of AFB1

A stock solution of AFB1 in methanol (1 mg mL^{-1}) was prepared and aliquots were diluted with PBS buffer yielding solutions from 0.25 to 10 ng mL^{-1}, which were used to obtain the calibration curve. In each measurement, 25 µL of AFB1 solution were dropped onto the working electrode. After incubation for 10 min, electrochemical impedance spectroscopy (EIS) and cyclic voltammetry (CV) measurements were performed using a hand-held potentiostat (PalmSens4, PalmSens BV, The Netherlands) controlled with PStouch app installed in a smartphone (Figure 1D). Prior to assessing the performance of the nanofiber-based immunosensor, the incubation time of antibody and antigen was carefully optimized. The EIS experiments were carried out by applying a voltage of 10 mV AC in the frequency range from 0.1 Hz to 10 kHz with an open circuit potential (OCP). The scanned potential range in the CV measurements was from −0.4 V to 0.4 V, and a 5 mM solution of ferri/ferrocyanide $[Fe(CN)_6]^{3-/4-}$ dissolved in 10 mM PBS solution (pH 7.4) was used. The same electrode was employed for the measurements of different AFB1 concentrations. In addition, the electrodes were washed with phosphate buffer between each standard point measurement, which was performed from low to high aflatoxin concentrations.

2.5 Application of the Immunosensors for Real Food Sample Analysis

Samples of grape juice and beer were purchased from a local market and prepared according to the literature [36]. Briefly, the samples of grape juice and beer were diluted 100-fold in deionized water and then spiked with AFB1 at concentrations varying from 0.25 to 10 ng mL^{-1}. The measurements were performed as described in section 2.3.

2.6 Data Analysis with Information Visualization Techniques

To study the selectivity of the sensing devices, statistical methods were applied to reduce the dimensionality of the data, allowing a visual representation in a 2-D projected space. Nyquist plots were analyzed using the Interactive Document Mapping (IDMAP) [37,38] technique within the Projection Explorer Sensors (PEx-Sensors) software [38]. In this multidimensional technique the Euclidean distances ($\delta(x_i,x_j)$) are calculated between datasets $X = \{x_1, x_2, \ldots, x_n\}$ with different AFB1 concentrations in the original space and projected into a lower-dimension space, where $Y = \{y_1, y_2, \ldots, y_n\}$ is the position of the visual elements and $d(y_i,y_j)$ is the Euclidean distance in this lower dimensional space. The "error" function that minimizes the term $|\delta(x_i, x_j) - d(f(x_i), f(x_j))| \; \forall \; x_i, x_j \in X$ is

given by eq. 1, where δ_{max} and δ_{min} are, respectively, maximum and minimum Euclidean distances.

$$Error_{IDMAP} = \frac{\delta(x_i, x_j) - \delta_{min}}{\delta_{max} - \delta_{min}} - d(y_i, y_j) \quad (1)$$

3 Results and Discussion

3.1 Fabrication of the Immunosensor and Detection Mechanisms

We investigated the electrospinning conditions of zein/PPy blend with a series of experiments at distinct voltages, polymer concentrations, and flow rates. Electrospinning of zein/PPy blends onto working electrodes appears to be the first in the literature. The surface morphology of the working electrode before and after nanofiber deposition with the optimized parameters from section 2.2 was analyzed with scanning electron microscopy (SEM). The images in Figure 2A and 2B show a heterogeneous surface for the non-modified electrode, which was entirely coated by uniform fibers with average diameter 465 ± 102 nm. Figures 2C and 2D indicate that the nanofiber morphology was preserved after anti-AFB1 immobilization and electrochemical measurements, confirming the nanofiber stability in aqueous media.

PM-IRRAS was utilized to investigate the immobilization of anti-AFB1 on zein/PPy nanofiber and the AFB1 detection mechanism. The spectra of pristine zein/PPy nanofiber and conjugated anti-AFB1 on zein/PPy nanofiber before and after AFB1 detection at a concentration of 10 ng mL^{-1} are shown in Figure 3. Zein/PPy nanofibers exhibited bands at 2875 cm^{-1} and 2960 cm^{-1} due to the asymmetric and symmetric C–H stretching from zein and PPy [39–41]. The bands at 1650 cm^{-1} and 1526 cm^{-1} are typical of zein, assigned to the stretching vibration of C=O in –CONH (amide I) and the N–H bending vibration (amide II), respectively [42,43]. The band at 1541 cm^{-1} is due to the pyrrole ring C=C and C–C stretching vibrations. The immobilization of anti-AFB1 mainly occurs via the covalent linkage between –NH_2 groups of zein with –COOH groups from anti-AFB1, leading to amide bonds [44]. Indeed, after attaching anti-AFB1 antibodies, the bands at 1650 cm^{-1} and 1526 cm^{-1} assigned to amide I and II appeared less intense and were shifted to lower wavenumbers. These changes are ascribed to the increase in oscillation energy of N–H/C–N dipoles and modification in orientation of N–H/C–N/C=O dipoles [45]. Further evidence of anti-AFB1 immobilization is provided by the reduction in band intensity at 1541 cm^{-1} possibly due to the intermolecular interaction

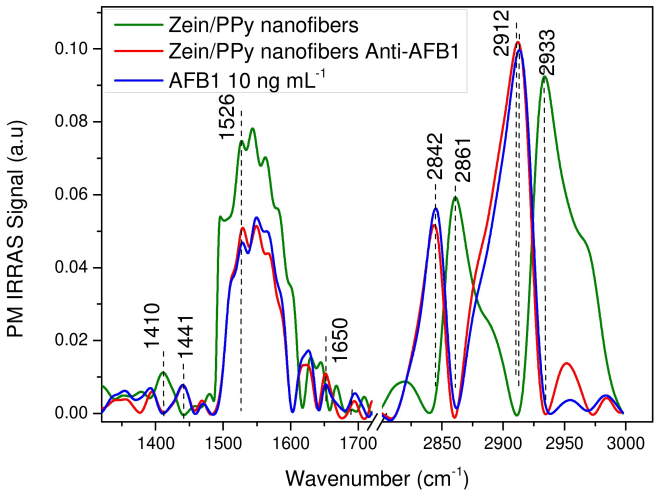

Fig. 3. PM-IRRAS spectra for PPy/Zein nanofibers, anti-AFB1 immobilized on PPy/Zein nanofibers, and after AFB1 detection (10 ng mL^{-1}) in the range 1376–1709 cm^{-1} and 2800–3000 cm^{-1}. The changes are ascribed to structural modifications on PPy/Zein nanofiber films.

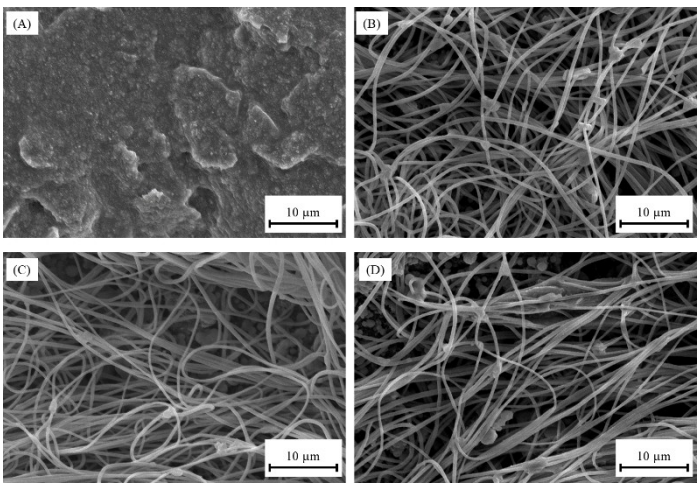

Fig. 2. SEM images of the non-modified working electrode (A); zein/PPy nanofibers deposited onto the working electrode (B); electrospun nanofibers after anti-AFB1 immobilization (C); coated electrode after electrochemical measurements (D).

between polypyrrole ring and anti-AFB1 antibodies. The mechanism responsible for AFB1 detection is also elucidated through the PM-IRRAS spectra. Changes in band intensity as the immunosensor is exposed to AFB1 can be caused either by adsorption or changes in the orientation of functional groups. When adsorption occurs the band intensity increases with the interaction between AFB1 mycotoxin and antibodies immobilized on the PPy/Zein nanofibers. On the other hand, reorientation of groups involved in the detection mechanism may cause a decrease in band intensity. Indeed, the bands due to amide I and II at 1650 cm^{-1} and 1526 cm^{-1}, respectively, are less intense after AFB1 detection. This indicates changes in orientation of amide I and II (N–H/C–N/C=O) dipoles from zein and anti-AFB1. A similar behavior was observed upon detecting distinct concentrations of AFB1 (Figures S1(A) and S1(B) in the Supplementary Material).

3.2 Detection of AFB1

The analytical performance of nanofiber-based electrochemical immunosensors was evaluated with Faradaic impedance measurements (in triplicate) using a redox pair ($[Fe(CN)_6]^{3-/4-}$). The Nyquist plots recorded after exposing the immunosensor to AFB1 solutions in Figure 4A were fitted using the Randle's equivalent circuit [46] in the inset. R_s is the electrolyte resistance, R_{ct} is the charge (electron) transfer resistance, C_{dl} is the interface capacitance, and Z_w is the Warburg impedance. The semicircular region at high frequencies is associated with interfacial charge transfer and its diameter corresponds to the charge transfer resistance (R_{ct}), while diffusion processes are ascribed to the linear region at low frequencies. Figure 4B shows the linear decrease in R_{ct} with the logarithm of AFB1 (log [AFB1]) concentration, with R_{ct} (Ohm) = 150.1–54.2 × log [AFB1] (ng mL^{-1}) being used to fit the data with a coefficient of determination (R^2) of 0.99. The limit of detection (LOD) was calculated from the ratio between the standard deviation (σ) of the response of three measurements (by using an AFB1 solution at fixed concentration (i.e., 0.25 ng mL^{-1}) and the slope (S) of calibration curve (LOD = 3.3 σ/S) resulting in a theoretical LOD = 0.092 ng mL^{-1}. We also calculated the limit of quantification (LOQ) (LOQ = 10(σ/S)) as 0.30 ng mL^{-1}. The maximum levels of ABF1 in food established by legislation from the European Union and the U.S. Food and Drug Administration (FDA) are 2 ng·mL^{-1} and 20 ng·mL^{-1}, respectively. In this regard, although theeoretical, the LOD and LOQ calculated indicate that the immunosensor presented here is adequate for monitoring AFB1 in food samples [47,48].

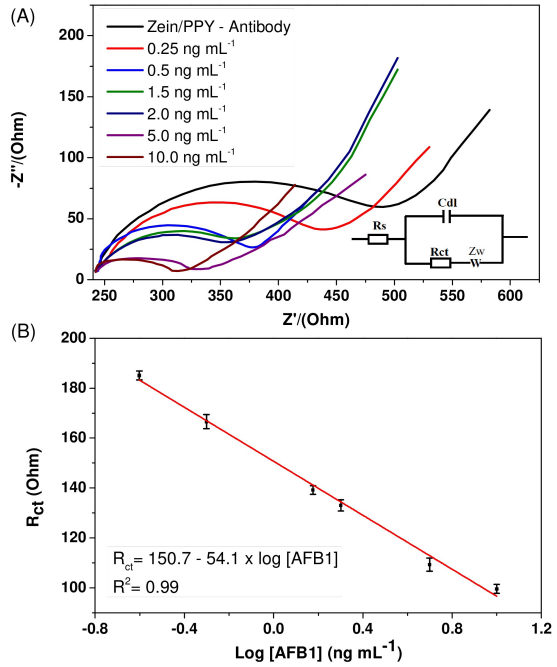

Fig. 4. (A) Nyquist plots of the electrochemical impedance measured with immunosensor comprising electrodes modified with Zein/PPy nanofibers in which anti-AFB1 was immobilized. Results are shown for the immunosensors exposed to distinct concentrations of AFB1 in standard solutions. The inset shows the equivalent circuit model used to fit the impedance data. (B) Rct × logarithm of AFB1 concentration from 0.25 to 10 ng mL^{-1}.

We have assessed the practical application of the nanofiber-based immunosensor to detect AFB1 in real samples of grape juice and beer. For this, we calculated the recovery rate (R (%)) by comparing the concentration values obtained from three experimental measurements of spiked samples and those theoretically determined from the calibration curve (R (%) = (experimental value/theoretical value) × 100 %) (Figure S2. and Table 1). As can be seen from Table 1, the recovery rate values indicate the accuracy and feasibility of the immunosensor.

We also confirmed the ability to discriminate the samples with distinct AFB1 concentrations by treating the Nyquist plots using the multidimensional projection technique IDMAP. The plots in Figure 5 show that the immunosensor was able to distinguish AFB1 traces in the three types of samples studied here: standard samples in buffer, and samples with AFB1 added to grape juice and beer. In addition to confirming the distinction ability, the plots show the data points with a tendency to be

Table 1. Recovery rate values (R (%)) for grape juice and beer samples spiked with distinct AFB1 concentrations.

Concentration	Sample Grape juice Recovery rate* (%)	 Beer Recovery rate (%)
0.25	98 ± 1	99 ± 2
1.0	97 ± 2	100 ± 1
1.5	99 ± 2	97 ± 1
2.0	100 ± 3	96 ± 3
2.5	98 ± 1	102 ± 2
5.0	96 ± 3	103 ± 1
10.0	99 ± 4	100 ± 4

* Results are represented as the mean ± standard deviation.

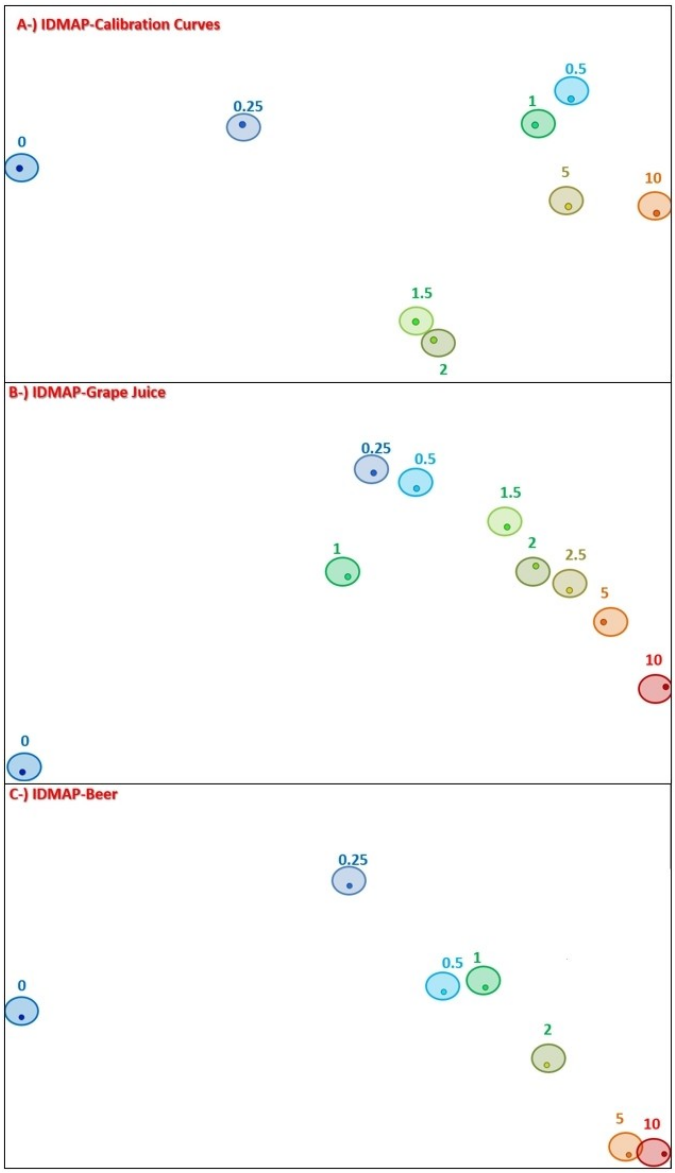

Fig. 5. IDMAP plots from the Nyquist data (Z''×Z') for AFB1 detection in: (A) standard samples, (B) grape juice and (C) beer. Note that the axes are not labeled because IDMAP calculates the relative Euclidean distances between samples with different AFB1 concentrations.

positioned to the right as the AFB1 concentration increases. The silhouette coefficient of each IDMAP projection was estimated by using the methodology proposed by Inselberg et al. [49], which quantifies the cohesion and separability of the different samples relying on calculated coefficient values ranging between [−1 and 1], where S ~ 1 indicates high distinction power between samples, while S ~ 0 and S ~ −1 correspond to neutral or low distinction power for such a distinction, respectively [49,50]. The calculated silhouette coefficients for samples $[Fe(CN)_6]^{3-/4-}$, grape juice and beer matrices were 0.536, 0.350, and 0.601, respectively, therefore confirming the high capability of proposed sensing platforms to detect AFB1 at different concentrations in distinct matrices, especially in beer samples.

The intra-electrode and inter-electrode reproducibility were calculated from three consecutive measurements at an AFB1 concentration of 0.25 ng mL^{-1} using the same electrode and distinct electrodes, respectively. The relative standard deviation (RSD) was 2.55 % for intra-electrode experiments and 3.42 % for the inter-electrode measurements. These low percentages indicate that the as-developed immunosensor can provide reproducible results. We also assessed the sensor stability after three weeks of storage at 4 °C using an AFB1 concentration of 0.25 ng mL^{-1}, which resulted in an experimental value of 0.25 ± 0.03 ng mL^{-1}, therefore indicating that the immunosensor detection efficiency was preserved. We compared the performance of the nanofiber-based immunosensor to other electrochemical immunosensors in the literature, as shown in Table 2. The detection limit (D.L.) of our immunosensor is comparable to some of the previous reports with the additional advantage of simplicity and low-cost of the fabrication process. In comparison with our previous work [15] in which the working electrode was modified with a film of chitosan/multiwalled carbon nanotubes (MWCNT), the nanofiber-based immunosensor presented here exhibited higher performance with a D.L. approximately seven times lower. This higher sensitivity is due to the intrinsic characteristics of electrospun nanofibers discussed in the introduction section.

The robustness of a biosensing platform depends on it not being affected by interfering compounds. An AFB1 immunosensor, for instance, must be able to distinguish it from other mycotoxins. In this study, we verified this selectivity with tests with ochratoxin A, another common mycotoxin found in food [10,15,33]. Electrochemical impedance spectroscopy data were obtained with the immunosensor exposed to different concentrations of

Table 2. Comparison of analytical performance of modified electrodes for detection of aflatoxin B1.

Immunoelectrode*	Linear range (ng mL^{-1})	Detection Limit (ng mL^{-1})	Ref.
BSA/anti-AFB1/Fe_3O_4–NFs/CNHs MGCE	0.05–200	0.02	[51]
BSA/anti-AFB1/nBi_2O_3/ITO	0.01–0.7	0.08	[52]
BSA/Anti-AFB1-chitosan/MWCNT	1–30	0.62	[15]
BSA/antiAFB1/SPA/3DTNEEs	0.004–6	0.001	[53]
BSA/anti-AFB1/Zein/PPy–NFs	0.25–10	0.092	This work

* BSA: bovine serum albumin Fe_3O_4–NFs: Fe_3O_4 nanoparticles incorporated into polymethylmethacrylate nanofibers; CNHs: Carbon horns on the magnetic electrode; MGCE: magnetic glassy carbon electrode; nBi_2O_3: bismuth oxide nanorods ITO: indium-tin oxide electrode; MWCNT: multiwalled carbon nanotubes functionalized with carboxylic acid; SPA: staphylococcus protein A; 3DTNEEs: gold three-dimensional nanotube ensembles.

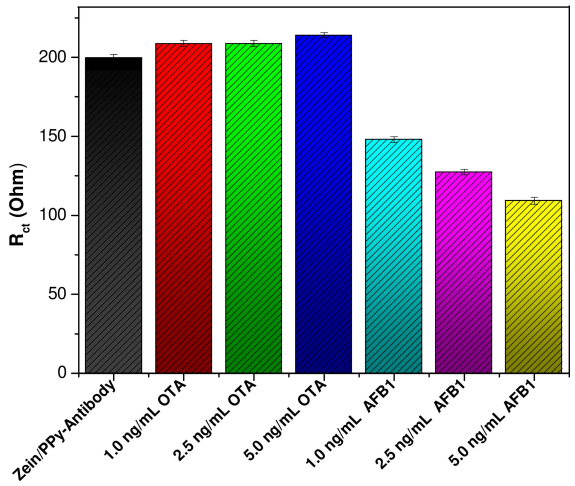

Fig. 6. Rct values for Zein/PPy-Antibody immunosensor before and after incubation with AFB1 and the interfering mycotoxin ochratoxin A (OTA).

ochratoxin A (OTA) and AFB1 (1, 2.5 and 5 ng mL^{-1}). The Rct values obtained from fitting the data with the equivalent circuit are shown in Figure 6. Since Rct did not change to any significant extent in the presence of different concentrations of OTA, one may infer the lack of interference.

4 Conclusions

We successfully fabricated a disposable zein/PPy nanofiber-based electrochemical immunosensor to detect AFB1 in varied food matrices, which can be employed with portable instruments for on-site analysis. The low-cost sensing platform displayed high sensitivity, wide detection range, and suitable limit of detection, in addition to requiring small amounts of material and being obtained with a simple process. Detection of AFB1 in real samples of grape juice and beer had recoveries of 98 % and 99 %, respectively. The selectivity of the immunosensor was confirmed with the IDMAP technique with plots indicating a clear distinction between different concentrations of AFB1 in real samples. The mechanism behind AFB1 sensing investigated using polarization-modulated infrared reflection absorption spectroscopy (PM-IRRAS) was found to be governed by specific interactions with changes in the orientation of the functional groups. In summary, the strategy adopted here is promising to generate a cost-effective, easy-to-use nanofiber-based immunosensor sufficiently robust to be handled by regular users for on-site AFB1 detection.

Acknowledgements

The authors acknowledge the financial support from Fundação de Amparo à Pesquisa do Estado de São Paulo (FAPESP) (2017/20973-4, 2017/21791-7, 2018/18953-8, 2017/12174-4, 2018/22214-6, 2020/14946-7), Conselho Nacional de Desenvolvimento Científico e Tecnológico (CNPq), INEO, MCTI-SisNano (CNPq/402287/2013-4), and Rede Agronano-EMBRAPA from Brazil.

Data Availability Statement

The data that support the findings of this study are available from the corresponding author upon reasonable request.

References

[1] H. Sohrabi, A. Hemmati, M. R. Majidi, S. Eyvazi, A. Jahanban-Esfahlan, B. Baradaran, R. Adlpour-Azar, A. Mokhtarzadeh, M. de la Guardia, *TrAC Trends Anal. Chem.* **2021**, *143*, 116344.
[2] S. Eyvazi, B. Baradaran, A. Mokhtarzadeh, M. de la Guardia, *Trends Food Sci. Technol.* **2021**, *114*, 712–721.
[3] L. A. Mercante, A. Pavinatto, T. S. Pereira, F. L. Migliorini, D. M. dos Santos, D. S. Correa, *Sensors and Actuators Reports* **2021**, 100048.
[4] C. Zhang, C. Jiang, L. Lan, J. Ping, Z. Ye, Y. Ying, *TrAC Trends Anal. Chem.* **2021**, *143*, 116369.
[5] O. S. Kwon, H. S. Song, T. H. Park, J. Jang, *Chem. Rev.* **2018**, *119*, 36–93.
[6] K. B. R. Teodoro, R. C. Sanfelice, F. L. Migliorini, A. Pavinatto, M. H. M. Facure, D. S. Correa, *ACS Sens.* **2021**, *6*, 2473–2496.
[7] R. Gupta, N. Raza, S. K. Bhardwaj, K. Vikrant, K. H. Kim, N. Bhardwaj, *J. Hazard. Mater.* **2021**, *401*, 123379.
[8] S. Kurbanoglu, C. Erkmen, B. Uslu, *TrAC Trends Anal. Chem.* **2020**, *124*, 115809.
[9] K. Yugender Goud, V. Sunil Kumar, A. Hayat, K. Vengatajalabathy Gobi, H. Song, K. H. Kim, J. L. Marty, *J. Electroanal. Chem.* **2019**, *832*, 336–342.
[10] A. Gevaerd, C. E. Banks, M. F. Bergamini, L. H. Marcolino-Junior, *Sens. Actuators B* **2020**, *307*, 127547.
[11] A. Smart, A. Crew, R. Pemberton, G. Hughes, O. Doran, J. P. Hart, *TrAC Trends Anal. Chem.* **2020**, *127*, 115898.
[12] F. Ma, L. He, E. Lindner, D. Y. Wu, *Appl. Surf. Sci.* **2021**, *542*, 148732.
[13] L. Shi, Z. Wang, G. Yang, H. Yang, F. Zhao, *Appl. Surf. Sci.* **2020**, *527*, 146934.
[14] V. T. Le, Y. Vasseghian, E. N. Dragoi, M. Moradi, A. Mousavi Khaneghah, *Food Chem. Toxicol.* **2021**, *148*, 111931.
[15] F. L. Migliorini, D. M. dos Santos, A. C. Soares, L. H. C. Mattoso, O. N. Oliveira, D. S. Correa, *Chemosensors* **2020**, *8*, 87.
[16] P. P. Mane, R. S. Ambekar, B. Kandasubramanian, *Int. J. Pharm.* **2020**, *583*, 119364.
[17] C. Cleeton, A. Keirouz, X. Chen, N. Radacsi, *ACS Biomater. Sci. Eng.* **2019**, *5*, 4183–4205.
[18] Y. Liu, M. Hao, Z. Chen, L. Liu, Y. Liu, W. Yang, S. Ramakrishna, *Curr. Opin. Biomed. Eng.* **2020**, *13*, 174–189.
[19] L. A. Mercante, V. P. Scagion, F. L. Migliorini, L. H. C. Mattoso, D. S. Correa, *TrAC Trends Anal. Chem.* **2017**, *91*, 91–103.
[20] M. Zhang, X. Zhao, G. Zhang, G. Wei, Z. Su, *J. Mater. Chem. B* **2017**, *5*, 1699–1711.
[21] L. Mascia, W. Zhang, F. Gatto, A. Scarpellini, P. P. Pompa, E. Mele, *ACS Appl. Polym. Mater.* **2019**, *1*, 1707–1716.
[22] L. Jing, X. Wang, H. Liu, Y. Lu, J. Bian, J. Sun, D. Huang, *ACS Appl. Mater. Interfaces* **2018**, *10*, 18551–18559.

[23] C. Ding, Y. Guo, J. Liu, G. B. Kent, B. T. Jobson, X. Fu, X. Yang, W. H. Zhong, *ACS Appl. Mater. Interfaces* **2020**, *3*, 2958–2964.
[24] C. M. Ewulonu, J. L. Chukwuneke, I. C. Nwuzor, C. H. Achebe, *Carbohydr. Polym.* **2020**, *235*, 116028.
[25] B. Ivanovics, G. Gazsi, M. Reining, I. Berta, S. Poliska, M. Toth, A. Domokos, B. Nagy, A. Staszny, M. Cserhati, E. Csosz, A. Bacsi, Z. Csenki-Bakos, A. Acs, B. Urbanyi, Z. Czimmerer, *J. Hazard. Mater.* **2021**, *416*, 125788.
[26] C. Budin, H. Y. Man, C. Al-Ayoubi, S. Puel, B. M. A. van Vugt-Lussenburg, A. Brouwer, I. P. Oswald, B. van der Burg, L. Soler, *Food Chem. Toxicol.* **2021**, *153*, 112258.
[27] M. Jia, X. Liao, L. Fang, B. Jia, M. Liu, D. Li, L. Zhou, W. Kong, *TrAC Trends Anal. Chem.* **2021**, *136*, 116193.
[28] K. Y. Goud, S. K. Kalisa, V. Kumar, Y. F. Tsang, S. E. Lee, K. V. Gobi, K. H. Kim, *Biosens. Bioelectron.* **2018**, *121*, 205–222.
[29] Z. Wu, H. Pu, D. W. Sun, *Trends Food Sci. Technol.* **2021**, *110*, 393–404.
[30] B. Huang, Z. Han, Z. Cai, Y. Wu, Y. Ren, *Anal. Chim. Acta* **2010**, *662*, 62–68.
[31] A. Y. Sirhan, G. H. Tan, R. C. S. Wong, *Food Control* **2013**, *31*, 35–44.
[32] S. Zhan, J. Hu, Y. Li, X. Huang, Y. Xiong, *Food Chem.* **2021**, *342*, 128327.
[33] C. Wang, Q. Zhao, *Biosens. Bioelectron.* **2020**, *167*, 112478.
[34] L. Yu, Y. Zhang, C. Hu, H. Wu, Y. Yang, C. Huang, N. Jia, *Food Chem.* **2015**, *176*, 22–26.
[35] H. Ma, J. Sun, Y. Zhang, C. Bian, S. Xia, T. Zhen, *Biosens. Bioelectron.* **2016**, *80*, 222–229.
[36] X. Lv, Y. Zhang, G. Liu, S. Wang, *RSC Adv.* **2017**, 16290–16294.
[37] R. Minghim, F. V. Paulovich, A. de Andrade Lopes, *Vis. Data Anal. 2006* **2006**, *6060*, 60600S.
[38] C. M. Daikuzono, F. M. Shimizu, A. Manzoli, A. Riul, M. H. O. Piazzetta, A. L. Gobbi, D. S. Correa, F. V. Paulovich, O. N. Oliveira, *ACS Appl. Mater. Interfaces* **2017**, *9*, 19646–19652.
[39] L. H. Daly, S. E. Wiberley, **2007**, *2*.
[40] M. E. Nicho, H. Hu, *Sol. Energy Mater. Sol. Cells* **2000**, *63*, 423–435.
[41] M. T. Ramesan, V. Santhi, *https://doi.org/10.1080/09276440.2018.1439626* **2018**, *25*, 725–741.
[42] X. Yu, C. Li, H. Tian, L. Yuan, A. Xiang, J. Li, C. Wang, A. V. Rajulu, *Chem. Eng. J.* **2020**, *396*, 125373.
[43] L. Deng, Y. Li, F. Feng, H. Zhang, *Food Hydrocolloids* **2019**, *87*, 1–10.
[44] W. V. K. Wheelwright, A. J. Easteal, S. Ray, M. K. Nieuwoudt, *J. Appl. Polym. Sci.* **2013**, *127*, 3500–3505.
[45] A. Wieckowski, C. Korzeniewski, B. Braunschweig, *Vib. Spectrosc.* **2013**, *4*, 1–423.
[46] Z. Wu, B. Wang, Z. Cheng, X. Yang, S. Dong, E. Wang, *Biosens. Bioelectron.* **2001**, *16*, 47–52.
[47] A. Krittayavathananon, M. Sawangphruk, *Anal. Chem.* **2017**, *89*, 13283–13289.
[48] M. Ren, H. Xu, X. Huang, M. Kuang, Y. Xiong, H. Xu, Y. Xu, H. Chen, A. Wang, *ACS Appl. Mater. Interfaces* **2014**, *6*, 14215–14222.
[49] A. Inselberg, B. Dimsdale, *Proc. First IEEE Conf. Vis. Vis. '90* n.d., 361–378.
[50] J. C. Soares, F. M. Shimizu, A. C. Soares, L. Caseli, J. Ferreira, J. Osvaldo N Oliveira, *ACS Appl. Mater. Interfaces* **2015**, *7*, 11833–11841.
[51] G. Xu, S. Zhang, Q. Zhang, L. Gong, H. Dai, Y. Lin, *Sens. Actuators B* **2016**, *222*, 707–713.
[52] P. R. Solanki, J. Singh, B. Rupavali, S. Tiwari, B. D. Malhotra, *Mater. Sci. Eng. C* **2017**, *70*, 564–571.
[53] X. Li, L. Cao, Y. Zhang, P. Yan, D. W. Kirk, *Electrochim. Acta* **2017**, *247*, 1052–1059.

Received: December 9, 2021
Accepted: May 17, 2022
Published online on ■■, ■■

RESEARCH ARTICLE

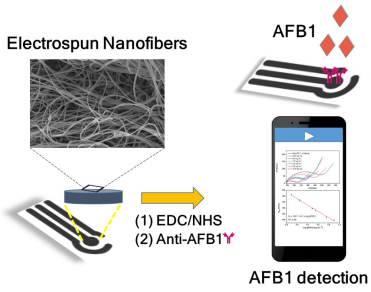

D. M. Dos Santos, F. L. Migliorini, A. C. Soares, L. H. C. Mattoso, O. N. Oliveira, Jr., D. S. Correa**

1 – 9

Electrochemical Immunosensor Made with Zein-based Nanofibers for On-site Detection of Aflatoxin B1